Statistical Analysis of Coherent Ultrashort Light Pulse CDMA With Multiple Optical Amplifiers Using Additive Noise Model

Kambiz Jamshidi and Jawad A. Salehi, *Member, IEEE*

***Abstract*—This paper describes a study of the performance of various configurations for placing multiple optical amplifiers in a typical coherent ultrashort light pulse code-division multiple access (CULP-CDMA) communication system using the additive noise model. For this study, a comprehensive performance analysis was developed that takes into account multiple-access noise, noise due to optical amplifiers, and thermal noise using the saddle-point approximation technique. Prior to obtaining the overall system performance, the input/output statistical models for different elements of the system such as encoders/decoders, star coupler, and optical amplifiers were obtained. Performance comparisons between an ideal and lossless quantum-limited case and a typical CULP-CDMA with various losses exhibit more than 30 dB more power requirement to obtain the same bit-error rate (BER). Considering the saturation effect of optical amplifiers, this paper discusses an algorithm for amplifiers' gain setting in various stages of the network in order to overcome the nonlinear effects on signal modulation in optical amplifiers. Finally, using this algorithm, various configurations of multiple optical amplifiers in CULP-CDMA are discussed and the rules for the required optimum number of amplifiers are shown with their corresponding optimum locations to be implemented along the CULP-CDMA system.**

***Index Terms*—Coherent ultrashort light pulse, femtosecond code-division multiple access (CDMA), multiple optical amplifiers, optical code-division multiple-access (OCDMA) technique.**

I. Introduction

RECENT studies for not-so-distant future Internet-based all-optical networks requirements with multimedia and broadband services are pointing toward a multiaccess technique that can operate without any network synchronization and provide secure access to its users without any delay. These requirements, along with some others, are most likely to be accommodated by all-optical code-division multiple-access (CDMA) techniques [1], [2].

Conceptually, categorizing these techniques leads to two main ideas for all-optical CDMA that is based on the type of source used for transmission, namely coherent and incoherent laser sources [3]–[10]. Although coherent techniques are more efficient than incoherent techniques [5], they are more complex when it comes to implementation, so there is a tradeoff between efficiency and complexity in implementing optical CDMA (OCDMA) systems.

Manuscript received June 19, 2004; revised January 18, 2005.

The authors are with the Electrical Engineering Department, Sharif University of Technology, Tehran 11365-9363, Iran (e-mail: jamshidi@mehr.sharif.edu; jasalehi@sharif.edu).

Digital Object Identifier 10.1109/JLT.2005.846903

One of the earliest coherent techniques that was introduced during the late 1980s is coherent ultrashort light pulse CDMA (CULP-CDMA) or femtosecond CDMA [11]. This technique can be considered as among the most advanced and promising OCDMA technique introduced to date with throughputs that can reach as high as hundreds of gigabits per second [4]. CULP-CDMA will soon enjoy the benefits of some recently invented and developed optical devices such as erbium-doped fiber amplifiers, arrayed-waveguide gratings, fiber Bragg gratings, semiconductor mode-locked lasers, all-optical thresholder, and dispersion compensation, in order to place itself amongst the most viable contenders in future all-optical (CDMA) networks [12]–[16]. These advances will undoubtedly help in the development of this technique in near future [17]. However, to further explore the potentials and efficiency of CULP-CDMA, a comprehensive study of the system performance using previously mentioned new devices is required. In particular, like any other optical multiaccess network based on a broadcasting architecture using passive star couplers, optical amplification in various points of the network may be required to compensate for the losses of splitting the encoded pulses and optical fiber path. Moreover, in order to meet the performance limits of the system at low input powers, we have to apply a proper gain setting algorithm, obtain the number of amplifiers required, and the best configuration for their placement within the network.

To study network performance for different optical amplifier configurations, we first model various key devices used in the network by obtaining the statistical relationship between the input and output amplitude of spectrally encoded pulses. Considering the effect of various devices that exist on the path from the source to the detector on the input pulse, we can obtain the statistics of photoelectrons liberated at the detector. Furthermore, we compute the bit-error rate (BER) of the system in the presence of multiuser interference, receiver thermal noise, and multiple optical amplifiers using the saddle-point approximation method. We then compare different architectures by using a different number of amplifiers in the system while imposing gain setting criteria in order to overcome the saturation effect of the amplifiers. It is important to highlight that our performance analysis does not take into account other imperfections and anomalies in a typical CULP-CDMA system such as timing jitter, encoder/decoder imperfections, nonlinearities, dispersion, and other effects.

The remainder of this paper is organized as follows. Section II gives a description of the CULP-CDMA system. Various devices, which are used in this technique, will be modeled in Sec-

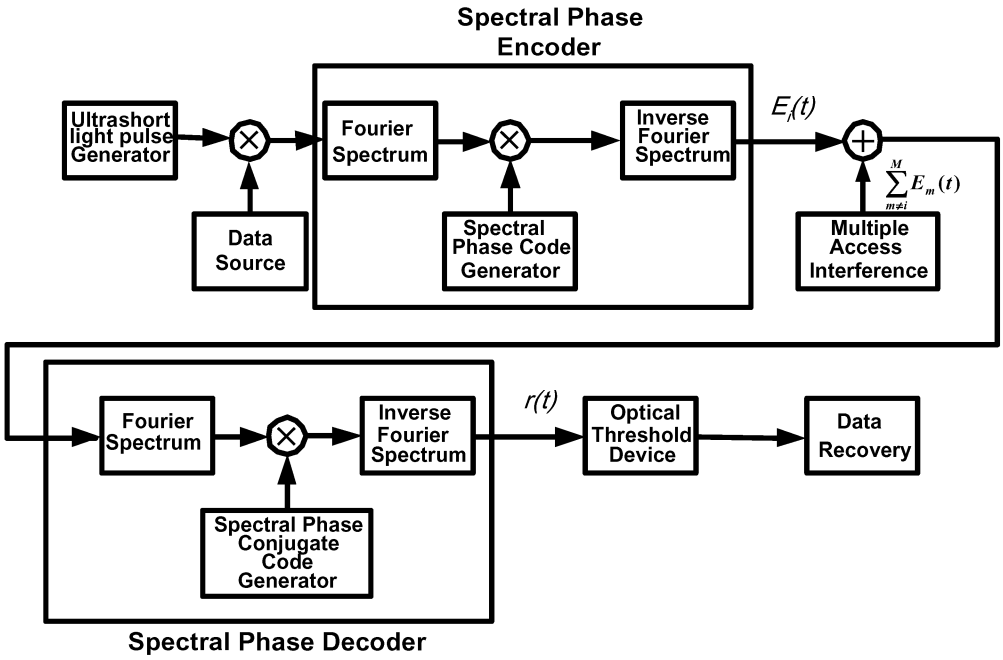

Fig. 1. Typical block diagram of a lossless CULP-CDMA system.

tion III. In Section IV analysis of the system for different amplifiers configurations will be presented, and the probability of error will be obtained. In Section V, numerical evaluation of the system performance for different structures will be given. We conclude the paper in Section VI.

II. System Description

Fig. 1 shows a typical lossless CULP-CDMA system. To encode the coherent pulse, the initial pulse spectrum is multiplied by a spectral phase code, which consists of $N_0 = 2N+1$ equal nonoverlapping frequency chips, where the value of frequency chips can be either -1 or 1. For this system, the electric field of the mth transmitted signal is approximately expressed as [4]

$$E_m(t) = \sum_{k=-\infty}^{\infty} d_k^{(m)} V_m(t - kT_b) \tag{1}$$

where $-T/2 < t < T/2, d_k^{(m)} \in \{0,1\}$ is the kth time slot data bit of the mth transmitted signal for binary ON–OFF keying (OOK) data source, and $V_m(t)$ is the encoded light pulse, which can be written as

$$V_m(t) = \frac{\sqrt{P_0}}{N_0} \sum_{n=-N}^{N} \exp\Big(-j\left(n\Omega t + \phi_n^{(m)}\right)\Big) \tag{2}$$

where P_0 is the peak power of the ultrashort light pulse and $\phi_n^{(m)} \in \{0, \pi\}$ denotes the nth code element of the mth user's transmitted signal. In the above equation, $\Omega = 2\pi/T$ is the width of the frequency chip and T is the duration of the transmitted pulse. For typical code values of -1 and 1, which corresponds to the phase values π and 0, respectively, we can choose maximal length shift register sequences, i.e., m-sequences, to encode the input light. It can be shown that for this case the optimum performance of the system will be achieved [4].

In this system, different users are assumed to be asynchronous, so the code-dependent part of the encoded light pulse with the initial transmission time t' can be written as [4]

$$V(t - t') = \alpha_x(t - t') - j\alpha_y(t - t') \tag{3}$$

where t' is defined on the interval $(-T_b/2 < t < T_b/2)$ and T_b is the bit period. In general, the period of data source T_b may be longer than the encoded pulse duration T, so a parameter K is defined to represent their ratio, i.e., $K = T_b/T$. In (3), $\alpha_x(t)$ and $\alpha_y(t)$ are the real and imaginary parts of $V(t)$ and are defined as [4]

$$\alpha_x(t - t') = \frac{\sqrt{P_0}}{N_0} \sum_{n=-N}^{N} \cos(n\Omega(t - t') + \phi_n + \theta) \tag{4}$$

$$\alpha_y(t - t') = \frac{\sqrt{P_0}}{N_0} \sum_{n=-N}^{N} \sin(n\Omega(t - t') + \phi_n + \theta). \tag{5}$$

Here, θ is the initial phase of the encoded signal and is defined on the interval $(-\pi, \pi)$. By choosing a random sequence (equal probability for $\varphi_n = 0$ and $\varphi_n = \pi$) for the code elements and assuming that θ and t' are uniformly distributed over their corresponding intervals, $\alpha_x(t - t')$ and $\alpha_y(t - t')$ can be modeled as a Gaussian process with the following joint probability density function (pdf) [4]:

$$P_{\alpha_x\alpha_y}(\alpha_x, \alpha_y, t) = \frac{1}{\pi(P_0/N_0)} \exp\left\{-\frac{(\alpha_x^2 + \alpha_y^2)}{P_0/N_0}\right\}, \quad N_0 \gg 1. \tag{6}$$

This equation shows that $\alpha_x(t - t')$ and $\alpha_y(t - t')$, the real and imaginary parts of the encoded signal, are statistically independent. Hence, the intensity of the light pulse has negative exponential probability density function [4] and the encoded light

pulse appears to be a random light when receiver has no knowledge of the code, time of transmission, and its initial phase [4].

The decoder for the mth receiver is similar to the mth transmitter's encoder, with a phase code that is complex conjugate of the transmitter code such that the mth decoder reconstructs the initial mth input light pulse. This decoder is not sensitive to the output of other encoders as long as their codes are not complex conjugate pair. Therefore, the intensity of the improperly decoded light pulse remains as a random light with a negative exponential function. The electric field of the output of the ith decoder is [4]

$$r(t) = E_{ii}(t) + \sum_{m \neq i}^{M} E_{mi}(t - t'_{mi}) \tag{7}$$

where M is the number of users. From (7), $r(t)$ can be written as the sum of two terms: the first term represents the properly decoded signal $E_{ii}(t)$ for the coherent input pulse, and the second term consists of improperly decoded pulses (multiple-access interference) $\sum_{m \neq i}^{M} E_{mi}(t - t'_{mi})$, which arises from other users' signal. In [4], it was shown that the statistics of the second term can well be approximated by two-dimensional Gaussian distribution.

III. Device Modeling

To analyze the performance of CULP-CDMA system with multiple optical amplifiers, we first need to obtain the pdf of the detected pulse. However, before we begin to obtain the pdf of the detected pulse, we begin by characterizing various optical devices used in CULP-CDMA system by obtaining their statistical input/output relationship.

A. Encoder/Decoder

To consider the effect of the encoder on the incident noise due to an optical amplifier, we first note that the relationship between power spectral densities at the input $(n(t))$ and output $(n'(t))$ of a system with frequency response equal to $G(f)$ can be written as

$$\Phi_{n'n'}(f) = \Phi_{nn}(f)|G(f)|^2 \tag{8}$$

where $\Phi_{nn}(f)$ is the power spectral density of the input noise and $\Phi_{n'n'}(f)$ is the power spectral density of the output noise. Since the code elements of the encoder accept values -1 and 1, the amplitude of the encoder's frequency response $|G(f)|$ is 1. This is valid for an ideal encoder. In general, the encoders are lossy elements with a loss equal to $\sqrt{L}$, i.e., $|G(f)| = \sqrt{L}$. If the variance of a random Gaussian light at the input of encoder is equal to N_{in} then the power spectral density of the output noise can be expressed as

$$\Phi_{n'n'}(f) = \Phi_{nn}(f)|G(f)|^2 = LN_{\text{in}}. \tag{9}$$

In general, the decoder affects each part of the received signal $r(t)$ in (7) separately and independently. The pulse of the kth transmitter, after passing through the kth decoder is decoded correctly and is converted back to the original coherent light pulse. The pulses of the other transmitters remain as pseudo-random noise with the same statistics as described in (6), [4].

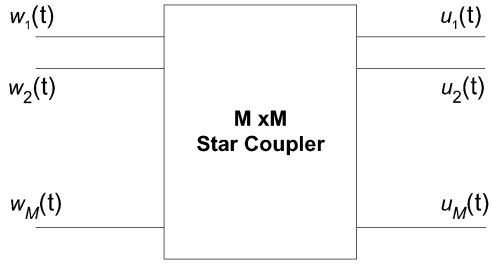

Fig. 2. Typical $M \times M$ star coupler: $u_i(t) = (1/\sqrt{M}) \sum_{k=1}^{M} e^{j\phi_{ik}} w_k(t)$.

The frequency response of the encoder and decoder are the same so the effect of the decoder on the amplifier's noise is similar to the effect of the encoder.

B. Star Coupler

An ideal star coupler combines the input fields of its input ports and divides each field equally among the output ports. Assume an $M \times M$ all-optical star coupler as in Fig. 2. Then, the input/output field amplitude relation can be written as [18]

$$u_i(t) = \frac{1}{\sqrt{M}} \sum_{k=1}^{M} e^{j\phi_{ik}} w_k(t) \tag{10}$$

where $u_i(t)$ is the sum of the input fields of the star coupler at its ith output port and $w_k(t)$ is the kth input port signal to the star coupler and ϕ_{ik} is the phase shift from kth input port to ith output port. We can obtain the variance of the output field versus that of the input fields of a star coupler as

$$\text{var}\{u_i(t)\} = \frac{1}{M} \sum_{k=1}^{M} \text{var}\{w_k(t)\}. \tag{11}$$

As it is seen in the above equation, the variance of the output signal is equal to the sum of the variances of the input signals. This is due to the independence of the input signals.

IV. Performance Analysis

Fig. 3 shows the block diagram of a typical CULP-CDMA system with multiple optical amplifiers. We analyze the performance of the system first by computing the effect of each user on the statistics of the output signal and second by obtaining the total statistics of the output signal.

In the following equations, it is assumed that L_1 and L_3 are losses due to encoder and decoder, and L_2 is the power loss of the optical fiber path. In addition, G_i is the gain of the ith amplifier, and M is the total number of users.

Using the results that were obtained in previous sections, and considering that the variance of the output of an amplifier is equal to the variance of the amplified input signal plus the intrinsic variance due to the amplifier itself, then the output of the second amplifier can be shown to be

$$w_i(t) = (\sqrt{G_1 G_2 L_1}) E_i(t) + X_i(t) \tag{12}$$

where $E_i(t)$ is the electric field of the ith transmitter as defined in (1), and $X_i(t)$ is the noise of the ith signal before entering the star coupler with a variance equal to

$$\text{var}(X_i(t)) = n_{\text{sp}}(G_1 - 1)L_1 G_2 + n_{\text{sp}}(G_2 - 1) \tag{13}$$

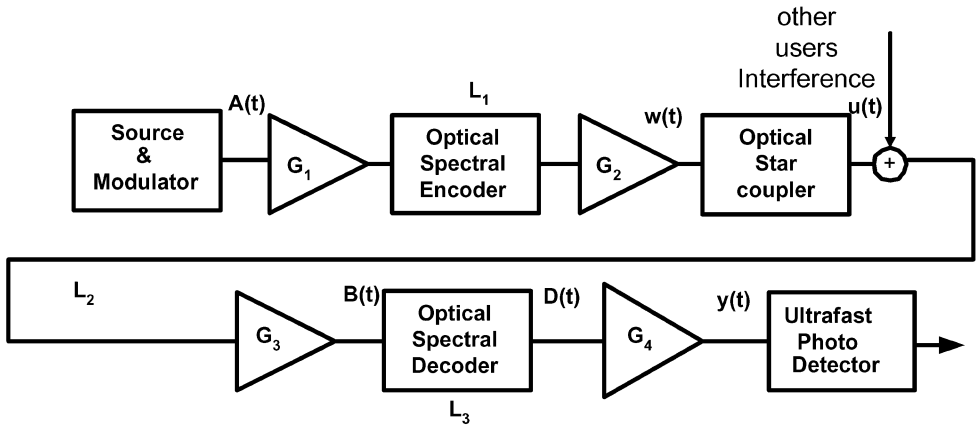

Fig. 3. System model representation for CULP-CDMA system with multiple optical amplifiers.

where $n_{\rm sp}$ is the spontaneous emission factor of the amplifier. The above variance is due to the noise of the first amplifier passing through the encoder (L_1) and the second amplifier, plus the additive intrinsic noise due to the second amplifier. According to (10) and (11) and considering the fact that the noise of each amplifier is independent of other amplifiers' noise, we can write the ith output of star coupler versus the input pulses as

$$u_i(t) = (\sqrt{G_1G_2L_1/M})\sum_{k=1}^{M} E_k(t) + Q_1(t). \quad (14)$$

Here, $Q_1(t) = (1/\sqrt{M})\sum_{i=1}^{M} X_i(t)$ is the noise of the signal after passing through the star coupler with variance equal to

$$\mathrm{var}(Q_1(t)) = n_{\rm sp}(G_1-1)L_1G_2 + n_{\rm sp}(G_2-1). \quad (15)$$

Note that the variance of the total amplifiers' noise (amplifier 1 and 2), (15), at each output port of the star coupler is equal to the input noise variance at each input port, (13). According to the input/ouput relation of amplifiers, one can write the input to the ith decoder as

$$B_i(t) = (\sqrt{G_1L_1G_2L_2G_3/M})\sum_{k=1}^{M} E_k(t) + Q_2(t). \quad (16)$$

In the above equation $Q_2(t)$ is the noise of the signal at the output of the third amplifier before entering the decoder with a variance equal to

$$\mathrm{var}(Q_2(t)) = n_{\rm sp}(G_1-1)L_1G_2L_2G_3 + n_{\rm sp}(G_2-1)L_2G_3 + n_{\rm sp}(G_3-1). \quad (17)$$

From (7), we can write the output pulse of the ith decoder as

$$D_i(t) = (\sqrt{G_1L_1G_2L_2G_3L_3/M})\left(E_{ii}(t) + \sum_{k=1,k\neq i}^{M} E_{ki}(t)\right) + Q_3(t) = (\sqrt{G_1L_1G_2L_2G_3L_3/M})r(t) + Q_3(t) \quad (18)$$

where $r(t), E_{ki}(t)$ and $E_{ii}(t)$ are defined in (7), and $Q_3(t)$ is the noise of the signal after passing through the decoder with a variance equal to

$$\mathrm{var}(Q_3(t)) = n_{\rm sp}(G_1-1)L_1G_2L_2G_3L_3 + n_{\rm sp}(G_2-1)L_2G_3L_3 + n_{\rm sp}(G_3-1)L_3. \quad (19)$$

Here, we can express the input pulse to the ith photodetector due to desired user and multiaccess users' transmitted pulses in CULP-CDMA as

$$y_i(t) = (\sqrt{G_1L_1G_2L_2G_3L_3G_4/M})r(t) + Q_4(t). \quad (20)$$

In this equation, $Q_4(t)$ is the noise of the signal before the photodetector with a variance equal to

$$\mathrm{var}(Q_4(t)) = n_{\rm sp}(G_1-1)L_1G_2L_2G_3L_3G_4 + n_{\rm sp}(G_2-1)L_2G_3L_3G_4 + n_{\rm sp}(G_3-1)L_3G_4 + n_{\rm sp}(G_4-1). \quad (21)$$

Detected signal variance is equal to the variance of $Q_4(t)$ plus the variance of $M-1$ other users' interfering signal. The undesired user's signal intensity is equal to the desired user's intensity attenuated by a factor N_0, so its variance is equal to P_0/N_0 with an equivalent photon number variance given by $(P_0T_c)/(N_0hf) = (m/N_0)$. Here, m is the average number of photons transmitted by each user, and f is the frequency of the encoded light pulse. We can rewrite the input pulse to the photodetector versus the transmitted pulses (by merging the second term of $r(t)$ ($M-1$ interfering signals) with the amplification noise $Q_4(t)$) as

$$y_i(t) = (\sqrt{G_1L_1G_2L_2G_3L_3G_4/M})E_{ii}(t) + Q_5(t) = \sqrt{G}E_{ii}(t) + Q_5(t) \quad (22)$$

where $G = (G_1L_1G_2L_2G_3L_3G_4/M)$ is the total gain of the system, and $Q_5(t)$ is the total input noise to the photodetector, and it is equal to the sum of the amplification noise and other users' interfering signal. Both of the above noise sources are Gaussian and independent, so the variance of $Q_5(t)$, i.e., N_T, is equal to the variance of the amplification noise plus the variance of the other users' interfering signal, i.e.,

$$\mathrm{Var}(Q_5(t)\,|\,U \text{ user sending data 1}) = N_T = n_{\rm sp}(G_1-1)L_1G_2L_2G_3L_3G_4 + n_{\rm sp}(G_2-1)L_2G_3L_3G_4 + n_{\rm sp}(G_3-1)L_3G_4 + n_{\rm sp}(G_4-1) + \frac{Um}{N_0\cdot M}G \quad (23)$$

where U is the number of active users, which transmit data bit 1.

For our performance analysis and for the sake of mathematical simplicity, we assume an ideal high-speed detector for the determination of the received signal. The detector indicates the intensity of incident light, so the decision variable is defined as

$$Y_i = \frac{1}{2}\int_0^{T_c} |\sqrt{G}E_{ii}(t) + Q_5(t)|^2\, dt. \tag{24}$$

Now, suppose that we can represent signal and noise in terms of their Fourier series as [19]

$$E_{ii}(t) = \sum_{n=-L}^{L} a_n e^{j2\pi nt/T} \tag{25}$$

$$Q_5(t) = \sum_{n=-L}^{L} q_n e^{j2\pi nt/T} \tag{26}$$

where a_n and q_n are Fourier coefficients of $E_{ii}(t)$ and $Q_5(t)$, and $2L+1$ is the number of signal modes. Then, the decision variable is simplified to

$$Y_i = \frac{T_c}{2}\sum_{n=-L}^{L} |\sqrt{G}a_n + q_n|^2. \tag{27}$$

The moment-generating functions of the above variable Y_i for transmitting 1 or 0 are

$$\Psi_0(z) = \frac{1}{(1+N_T\eta(1-z))^{2L+1}} \tag{28}$$

$$\Psi_1(z) = \frac{1}{(1+N_T\eta(1-z))^{2L+1}} \exp\left(\frac{-mG\eta(1-z)}{1+N_T\eta(1-z)}\right) \tag{29}$$

where N_T is the total noise variance of the detected signal as in (23), m is the average number of photons transmitted by the desired user for data bit 1, and η is the quantum efficiency of the detector. We note that this moment-generating function is obtained for the system if there are U interfering users.

After detection, thermal Gaussian noise is added to the detected electrical signal. Therefore, the distribution of the output signal from the detector is the convolution of a noncentral negative binomial distribution and a Gaussian distribution, which can be written in the form of the moment-generating function as

$$\Phi_l(s) = \Psi_l(e^s)\exp\left(\frac{\sigma_{\text{th}}^2}{2}s^2\right), \quad l = 0, 1 \tag{30}$$

$$\sigma_{\text{th}}^2 = \frac{2\cdot k_B\cdot T_r\cdot T_c}{R_L\cdot e^2}. \tag{31}$$

Here, σ_{th}^2 is the power of thermal noise, k_B is the Boltzman constant, T_r is the equivalent temperature of the receiver, e is the charge of the electron, and R_L is the resistance of the load, which is seen from the receiver input. The pdf $P_v(v)$ associated with liberated photoelectrons from the detector and the additive thermal noise is equal to the inverse Fourier transform of $\Phi_l(s)$.

The probability of error for this system as shown in [4] is equal to

$$P(\text{error}) = \sum_{i=1}^{M-1} P(\text{error}\,|\,i)P(i) \tag{32}$$

where $P(\text{error}\,|\,i)$ is the probability of error if there are i interfering users that are transmitting data bit 1 in the same slot that the main user transmits data, and $p(i)$ is the probability of the presence of i interfering users. Assuming $M-1$ interfering users, the probability that there are i users that transmit data on the desired pulse is [4]

$$P(i) = \binom{M-1}{i}\left(\frac{1}{2K}\right)^i\left(1-\frac{1}{2K}\right)^{M-1-i} \tag{33}$$

where K is defined in Section II and is equal to the ratio of the bit period to the encoded pulse duration. For obtaining $P(\text{error}\,|\,i)$, we have

$$\begin{aligned} P(\text{error}\,|\,i) &= \frac{1}{2}[P(\text{error}\,|\,i,0) + P(\text{error}\,|\,i,1)] \\ &= \frac{1}{2}\left[\int_{\text{Th}}^{\infty} P_v(v\,|\,i,0)\, dv + \int_{-\infty}^{\text{Th}} P_v(v\,|\,i,1)\right] \end{aligned} \tag{34}$$

where $P(\text{error}\,|\,i,l)$ is the probability of error if there are i users to interfere, the transmitted signal is $l \in \{0,1\}$, and $P_v(v\,|\,i,l)$ is the pdf of the output photoelectrons plus the thermal noise if there are i interfering users. Here, we define Th as the threshold and is selected such that it minimizes the probability of error. If the received signal exceeds the threshold level Th, the data bit is considered as 1; otherwise, it is recognized as 0. In obtaining the probability of error for this system, we choose a method based on saddle-point approximation [19]. According to [19], a new function is defined as $\Gamma_l(s) = \ln(\Phi_l(s)e^{-\text{Th}\cdot s})/(s)$. If the positive root of equation $\Gamma_0'(s) = 0$ is called s_0 and negative root of equation $\Gamma_1'(s) = 0$ is called s_1, the saddle-point approximation states that [19]

$$\begin{aligned} \int_{\text{Th}}^{\infty} P_v(v\,|\,i,0)\, dv &\approx \frac{\exp(\Gamma_0(s_0))}{\sqrt{2\pi\Gamma_0''(s_0)}} \\ \int_{-\infty}^{\text{Th}} P_v(v\,|\,i,1)\, dv &\approx \frac{\exp(\Gamma_1(s_1))}{\sqrt{2\pi\Gamma_1''(s_1)}}. \end{aligned} \tag{35}$$

By using (28)–(35), we can approximate the error probability of the system.

V. Numerical Results

In our numerical analysis, we use the following parameters, as shown in Table I, for a typical CULP-CDMA. The noise due to dark current is neglected in our analysis since the time of integration is too short. Fig. 4 shows the probability of error for the ideal and quantum-limited cases. For the ideal case, we neglect the shot noise effect. In the quantum-limited case, thermal noise is also neglected. The system is assumed to be lossless in both cases, i.e., $G = 1/M$. Fig. 4 indicates that by increasing the number of photons, the quantum-limited case approaches the ideal case. By transmitting 5000 photons in a pulse, one can reach a probability of an error as low as 2×10^{-8} for the system parameters given in Table I.

TABLE I
TYPICAL VALUES USED IN THIS PAPER

N_0	*Code Length*	*128*
M	*Number of Users*	*20*
R	*Bit Rate*	*400 Mbps*
$G_{\max}$	*Max. Gain of each Amplifier*	*1000 (30dB)*
n_{sp}	*Spontaneous Emission Factor*	*1.1*
T_r	*Receiver Temperature*	*300 K*
A_f	*Fiber Area*	*1 e –10 m^2*
R_L	*Load Resistance*	*1000 Ω*
i_d	*Dark current*	*1 e –10 A*
T_c	*width of ultrashort pulse*	*80fsec*
ϕ_s	*Saturation Flux Density*	*1e27 photon/sec.m^2*
η	*Quantum Efficiency*	*0.8*
$L_1(L_3)$	*Encoder(Decoder) Loss*	*7dB*
L_2	*Path Loss*	*10dB*

Fig. 5 shows bit-error probability for a typical system without the amplifier. For this case, we consider the effect of various losses in the network and thermal noise on the performance of the system. It is apparent that by transmitting 5×10^6 photons in a pulse, i.e., 1000 times (30 dB) that of the quantum-limited case, one can reach an error probability equal to 2×10^{-8}. We combat this difference by using optical amplifiers in the network.

The main issue for assigning gain values to optical amplifiers is due to their corresponding saturation effect. Saturation occurs when the ratio of the input photon number to the amplifier exceeds a threshold. This threshold should be selected in such a way that the amplifier operates in its linear regime, and it is customary to choose the average number of the output signal photons to be below $0.1\phi_s A_f T$ where, A_f is the fiber area and ϕ_s is the saturation photon flux density [20]. The value of the fiber effective area is assumed to be 10^{-11} m^2. In this paper, we choose an algorithm similar to [20]. In this method, each amplifier operates in the linear regime by restricting the average number of photons in each pulse to be below the saturation threshold; then, the maximum achievable gain is assigned to each amplifier. This gain is the minimum value between the allowed gain due to the saturation restriction and the maximum gain for a typical optical amplifier. It means that the gain values can be set to a maximum number between 1 and 1000 (the maximum gain considered for the amplifier in the text) if the output number of photons from the amplifier does not exceed $0.1\phi_s A_f T$.

Since the threshold of saturation is proportional to the time duration of input signal, the amplifiers, which are placed in the middle stages of the system, have larger saturation threshold. The saturation level for the G_1 and G_4 amplifiers in this typical system with the parameters specified in Table I is equal to 4000 photons, which means that the number of photons at the output of these amplifiers cannot exceed 4000 photons. This number of photons corresponds to a peak power of 1.27 mw. The saturation level for the G_2 and G_3 amplifiers is equal to 512 000 photons. This value corresponds to the same level of peak power due to the broadening of the encoded light pulse. As seen in Fig. 3, the amplified encoded pulse will be transmitted through the fiber. Its time duration is about 51.2 ps, and its maximum power is 1.27 mW. Using these parameters, we can neglect the nonlinear effects of the fiber on the pulse shape [13]. We should note that we assume that dispersion does not affect the performance of the system i.e., a dispersion compensation technique is used to eliminate the effect of dispersion [21].

Using the previously mentioned algorithm, the BER for the systems with one to four amplifiers is obtained using saddle-point approximation, and the results are sketched in the Figs. 6, 8, 9, and 11. It can be seen that the performance of the system when using the optical amplifier approaches that of quantum-limited performance. In addition, the gain values of optical amplifiers for the important configurations are sketched in Figs. 7, 10, and 12. As can be seen in these figures, saturation of optical amplifiers depends on the transmitted peak pulse, duration of traversing pulse, and the amount of loss and gain prior to their input.

If there is only one amplifier in the system as it is seen in Fig. 6, then the amplifier denoted as (G_2), i.e., the second amplifier in Fig. 3, achieves the best performance, while (G_3) achieves a better performance than both (G_1) and (G_4). In general (G_2) and (G_3) amplifiers have higher saturation threshold, as described above, than (G_1) and (G_4) amplifiers, so they can have more gains than the other two configurations, causing them to perform better in this system. (G_2) performs better than the (G_3) amplifier due to the fact that under equal circumstances, the postamplifier configuration usually operates better than the preamplifier configuration [20]. However, this is not the usual case when considering the saturation effect of the amplifiers. As it is seen in Fig. 6, the performance of the system with the first amplifier (G_1) is the worst compared with the other three configurations.

In Fig. 7, the values of amplifier gains are shown for one-amplifier configurations. In these configurations, at first G_1 amplifier saturates, after that G_2 and then G_4, will reach saturation level. The G_3 amplifier will not be saturated if it is used alone in the configuration. The gain of the first amplifier reaches 1 by increasing the transmitted power. Due to our gain-setting algorithm, the value is set to 1, i.e., there is no amplification, if the input power to the amplifier exceeds the saturation threshold. This effect occurs for the first and fourth amplifier when there are 4000 photons at their output or there are 512 000 photons at the output of second and third amplifiers. This is the origin of the breaking point, which will be seen in Figs. 8 and 11, where we have considered the performance of the system. In that power region, G_1 enters highly saturated regime, and as will be seen in Fig. 11, the performance of systems that do not use G_1 in their configuration reaches those systems using G_1. Due to the gain-setting algorithm, when more than one amplifier is used, amplification in the early stages of the configuration causes the following amplifiers into saturation level, as will be

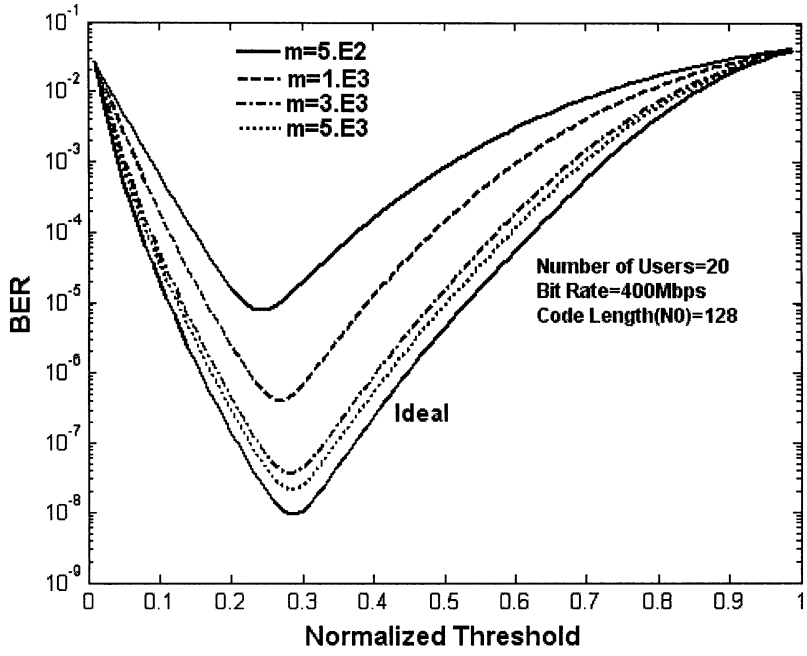

Fig. 4. BER versus normalized threshold for ideal and quantum-limited cases.

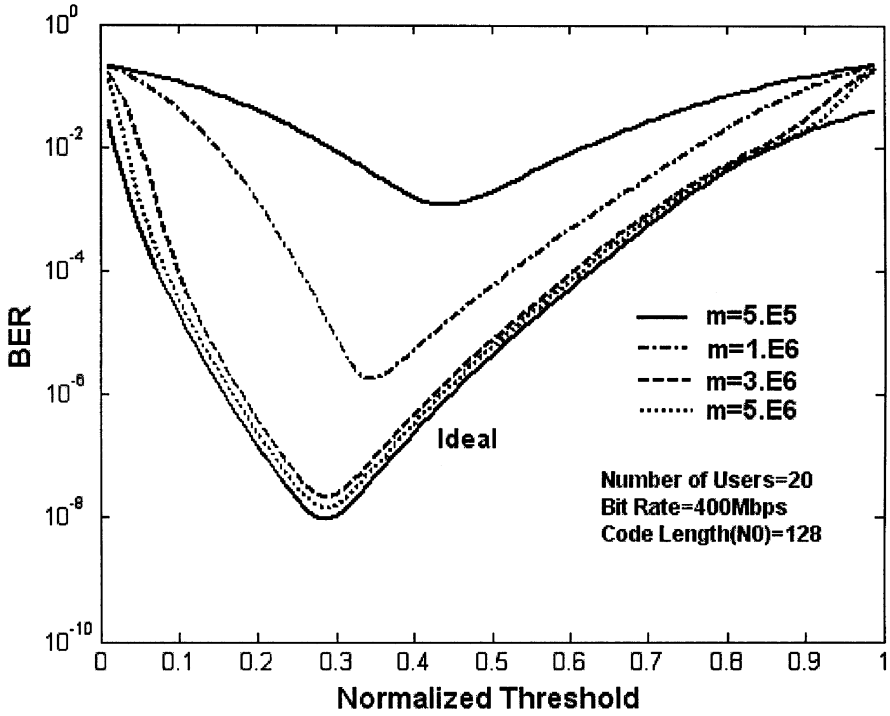

Fig. 5. BER versus normalized threshold for ideal case and a typical system without amplifiers.

seen in Figs. 10 and 12. This fact causes each following amplifiers' gain to be affected by the previous amplifiers' gain setting. However, for the first amplifier, the gain could remain fixed since it is not followed by any preceding amplifier.

The performance of the two amplifiers configurations is sketched in Figs. 8 and 9. As it is seen in these figures, (G_1, G_2) and (G_2, G_3) configurations are the best configuration among two-amplifier systems. The performance of the system that uses the (G_1, G_2) configuration is superior to other configurations when transmitted source power is low. However, by increasing the transmitted power, the first amplifier reaches its saturation regime, i.e., the transmitted power into the G_1 amplifier exceeds its saturation power, so due to our gain-setting algorithm, its gain is set to 1, and it would not have any effect on the performance of the system. As it is seen in Fig. 8, the performance of the (G_2, G_3) configuration is slightly better than the performance of the (G_1, G_2) as the transmitted power is increased and ultimately reaches the performance of four-amplifier configuration. (G_1, G_4) has the worst performance in the two-amplifier configurations; this is due to the fact that G_1

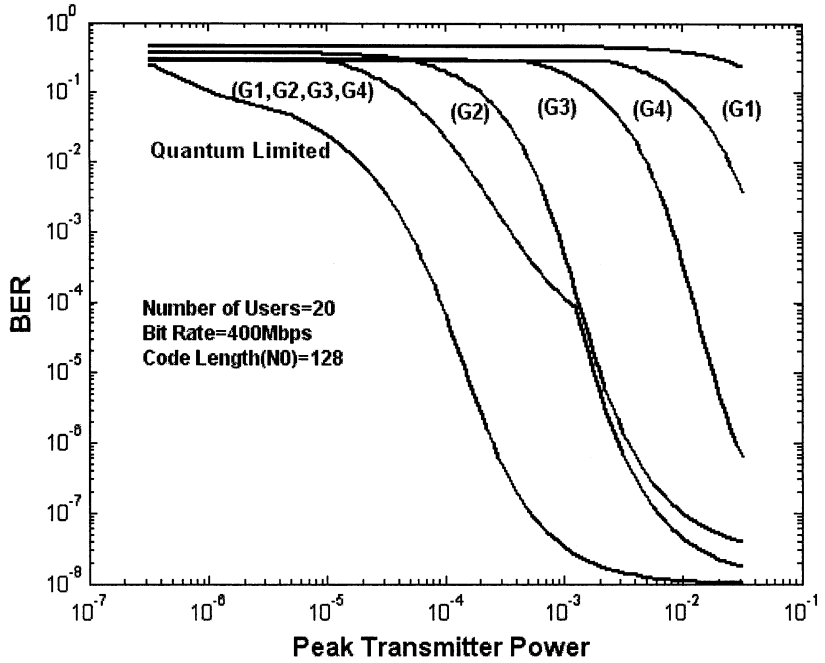

Fig. 6. BER versus peak transmitter power for quantum-limited case, and a typical system with one amplifier or four amplifiers.

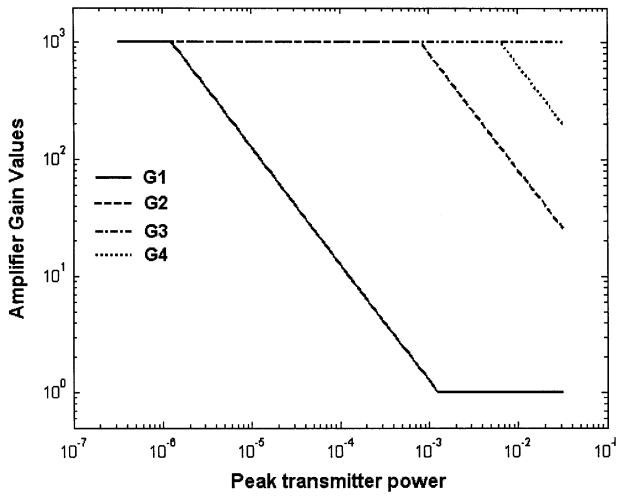

Fig. 7. Amplifier gain values versus peak transmitter power for one amplifier system.

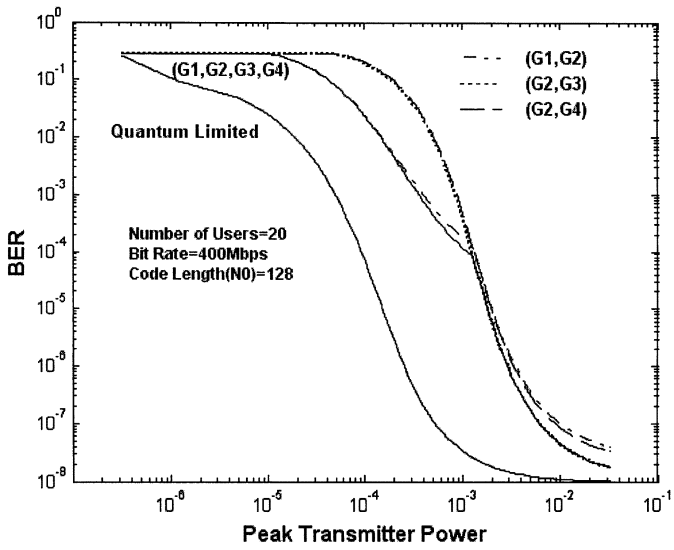

Fig. 8. BER versus peak transmitter power for quantum-limited case, and a typical system with two and four amplifiers.

suffers from a low-saturation regime and G_4 suffers from a low signal-to-noise ratio; hence, the combined configuration gives the worst possible performance (see Fig. 8).

In Fig. 10, the value of the amplifier gains are shown in two of the best two-amplifier configurations, i.e., $(G_1, G_2), (G_2, G_3)$. It can be seen that the gain of the G_1 amplifier decreases by increasing the input pulse power until it reaches 1 at the breakpoint. Therefore, one can conclude that the (G_1, G_2) configuration performs better than the (G_2, G_3) configuration before breakpoint, as seen from Fig. 8. As can be seen in this figure, after breakpoint, due to the saturation of the first amplifier, the gain of the second amplifier will be the same for both configurations. Due to the gain setting of the third amplifier, the (G_2, G_3) configuration has better performance than the (G_1, G_2) configuration, which is in line with the BER of the systems, as discussed in Fig. 8.

For the three-amplifier case, the best amplifier placement is the (G_1, G_2, G_3) configuration (Fig. 11). It is seen in Fig. 11 that the probability of error for the (G_1, G_2, G_3) configuration is extremely close to the performance of the four-amplifier configuration (G_1, G_2, G_3, G_4). This is due to the saturation effect of the first amplifier, which can be observed in Fig. 7. Comparing the (G_1, G_2, G_3) with the (G_2, G_3) configuration indicates that their difference is only in the low-power regime, and this difference is mainly due to the effect of the G_1 amplifier. The performance of both configurations is equal when the G_1 amplifier is in its saturation level, which is shown in Fig. 12. In Fig. 11 and others, the breaking point in the performance curves are due to the saturation effect of the G_1 amplifier beyond which the gain of G_1 amplifier is reduced to 1(0 dB).

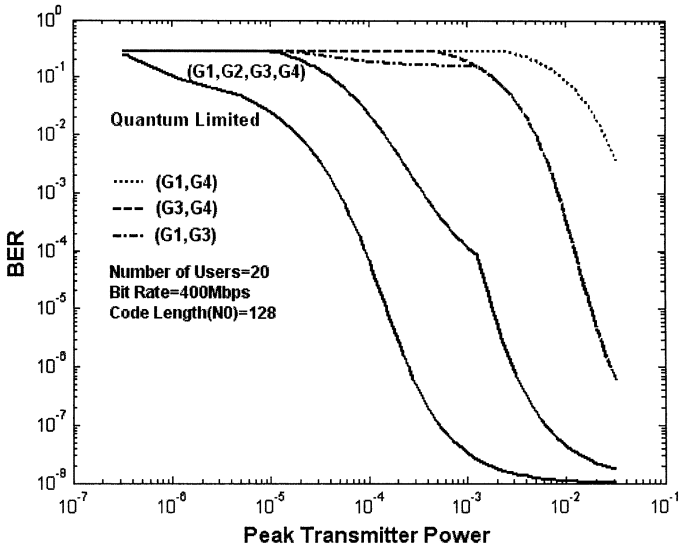

Fig. 9. BER versus peak transmitter power for quantum-limited case, and a typical system with two and four amplifiers.

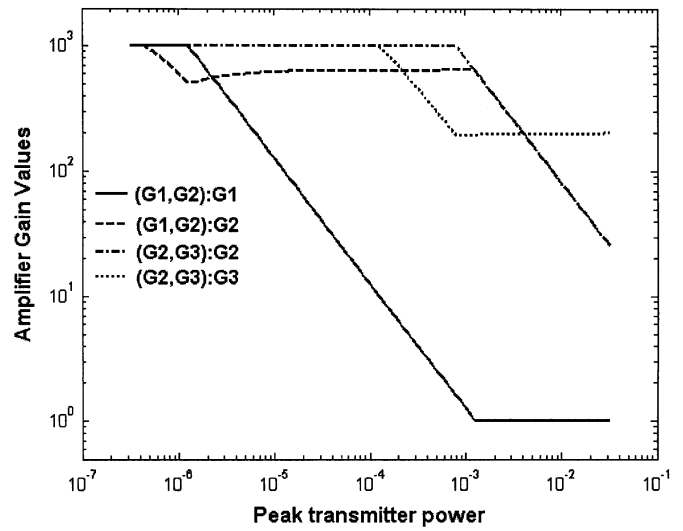

Fig. 10. Amplifier gain values versus peak transmitter power for two types of two-amplifier systems.

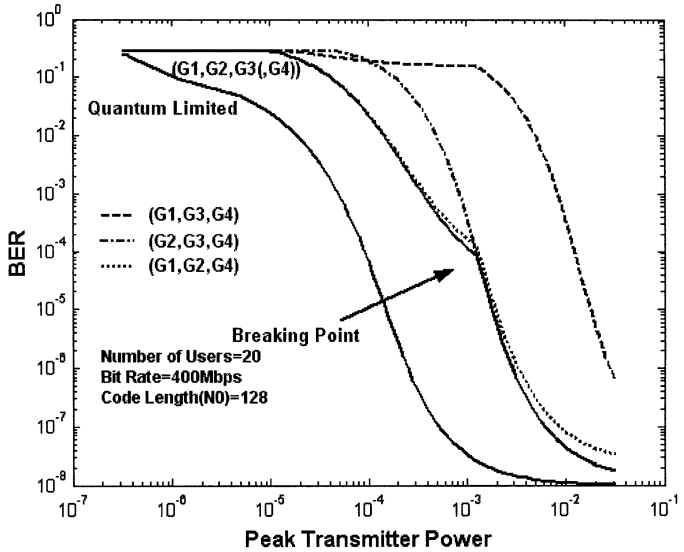

Fig. 11. BER versus peak transmitter power for quantum-limited case, and a typical system with three and four amplifiers. The breaking point in the above curve is due to the saturation effect of G_1 beyond which the gain of the first amplifier G_1 is set to unity, i.e., 0-dB gain.

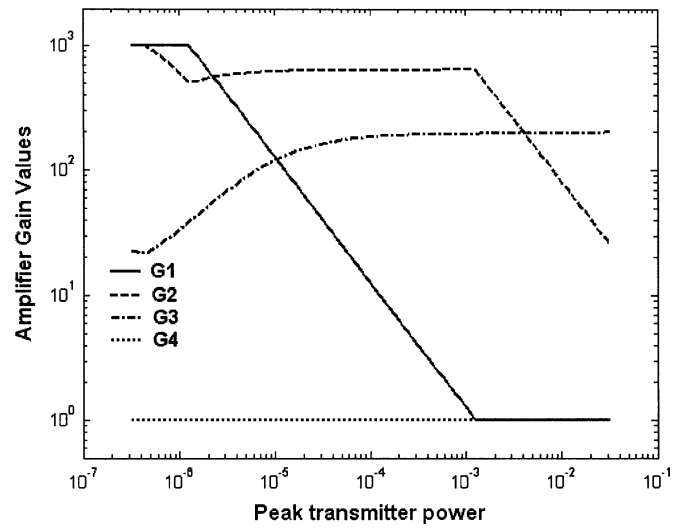

Fig. 12. Amplifier gain values versus peak transmitter power for four amplifier system, i.e., (G_1, G_2, G_3, G_4).

In Fig. 12 the value of amplifier gains are shown in four-amplifier configuration, i.e., (G_1, G_2, G_3, G_4). As seen in this figure, the fourth amplifier always operates in the saturation regime, and its gain is set to 1, and the gain of the first amplifier is set to 1 after the breakpoint as well. This confirms the results obtained in Fig. 11 that the performance of the (G_1, G_2, G_3) configuration is equal to the performance of the four-amplifier configuration. It also confirms the result obtained in Fig. 8 that in high-power regime, after breakpoint, the (G_2, G_3) configuration has a performance equal to the four-amplifier configuration.

From the above discussions, one can deduce that choosing G_2 is best when one considers one-amplifier configuration. However, if we want to use a two-amplifier configuration, then it is best to choose the (G_1, G_2) configuration in the low-power regime and the (G_2, G_3) configuration in the high-power regime.

To obtain amplifier gain values for the (G_1, G_2, G_3, G_4) configuration at peak power 10^{-4}, for example, a line parallel to the vertical axis is drawn, and the intersection of this line with other curves indicates the gain value for that amplifier. For this example, at $P_0 = 10^{-4}, G_4 \cong 1$ (0 dB), $G_3 \cong 200$ (23 dB), $G_2 \cong 600$ ($\cong$27 dB), and $G_1 \cong 20$ (13 dB).

VI. Conclusion

This paper discussed and analyzed the performance of a coherent ultrashort light pulse code-division multiple-access (CULP-CDMA) system with multiple optical amplifiers. A comparison between the quantum-limited case and a typical system exhibits about 1000 times difference in average photon number required for the same probability of error. This difference in input photon number approaches zero by using optical amplifiers. Performance analysis was done for different configurations of optical amplifiers. It is shown that by placing optical amplifiers in the second and third stages, i.e., (G_2, G_3),

system performance is better than placing them in the first and fourth stages, i.e., (G_1, G_4). Finally, the second amplifier G_2 has the best performance under various conditions.

REFERENCES

[1] J. Ratnam, "Optical CDMA in broadband communication-scope and applications," *J. Op. Commun.*, vol. 23, no. 1, pp. 11–21, 2002.

[2] A. Stok and E. H. Sargent, "The role of optical CDMA in access networks," *IEEE Commun. Mag.*, vol. 40, no. 9, pp. 83–87, Sep. 2002.

[3] J. A. Salehi, "Code division multiple-access techniques in optical fiber network—Part I: Fundamental principles," *IEEE Trans. Commun.*, vol. COM-37, no. 8, pp. 824–833, Aug. 1989.

[4] J. A. Salehi, A. M. Weiner, and J. P. Heritage, "Coherent ultrashort light pulse code-division multiple access communication systems," *J. Lightw. Technol.*, vol. 8, no. 3, pp. 478–491, Mar. 1990.

[5] M. E. Marhic, "Coherent optical CDMA networks," *J. Lightw. Technol.*, vol. 11, no. 5/6, pp. 854–864, May/Jun. 1993.

[6] R. A. Griffin, D. D. Sampson, and D. A. Jackson, "Coherence coding for photonic code-division multiple access networks," *J. Lightw. Technol.*, vol. 13, no. 9, pp. 1826–1837, Sep. 1995.

[7] H. Fathallah, L. A. Rusch, and A. LaRochelle, "Passive optical fast frequency-hop CDMA communications system," *J. Lightw. Technol.*, vol. 17, no. 3, pp. 397–405, Mar. 1999.

[8] A. J. Mendez, R. M. Gagliardi, H. X. C. Feng, J. P. Heritage, and J.-M. Morookian, "Strategies for realizing optical CDMA for dense, high-speed, long span, optical network applications," *J. Lightw. Technol.*, vol. 18, no. 12, pp. 1685–1696, Dec. 2000.

[9] A. Pe'er, B. Dayan, Y. Silberberg, and A. A. Friesem, "Optical code-division multiple access using broad-band parametrically generated light," *J. Lightw. Technol.*, vol. 22, no. 6, pp. 1463–1471, Jun. 2004.

[10] S. Yegananarayanan, A. S. Bhushan, and B. Jalali, "Fast wavelength-hopping time-spreading encoding/decoding for optical CDMA," *IEEE Photon. Technol. Lett.*, vol. 12, no. 5, pp. 573–575, May 2000.

[11] J. A. Salehi, A. M. Weiner, and J. P. Heritage, "Introducing femtosecond optical code division multiple access networks," in *IEEE Int. Symp. Information Theory*, vol. 88, IEEE Catalog No. CH 2621-1, 1988, p. 220.

[12] K. S. Kim, D. M. Marom, L. B. Milstein, and Y. Fainman, "Hybrid pulse position modulation/ultrashort light pulse code-division multiple-access systems—Part II: Time-space processor and modified schemes," *IEEE Trans. Commun.*, vol. 51, no. 7, pp. 1135–1148, Jul. 2003.

[13] H. P. Sardesai, C.-C. Chang, and A. M. Weiner, "A femtosecond code-division multiple-access communication system test bed," *J. Lightw. Technol.*, vol. 16, no. 11, pp. 1953–1964, Nov. 1998.

[14] H. Tsuda, H. Takenouchi, T. Ishii, K. Okamoto, T. Goh, K. Sato, A. Hirano, T. Kurokawa, and C. Amano, "Spectral encoding and decoding of 10 Gbit/s femtosecond pulses using high resolution arrayed-waveguide grating," *Electron. Lett.*, vol. 35, no. 14, pp. 1186–1188, Jul. 1999.

[15] Z. Zheng, H. Sardesai, C. C. Chang, A. M. Weiner, J. H. March, and M. M. Karkhanehchi, "Nonlinear detection of spectrally coded ultrashort pulse by two-photon absorption GaAs waveguide photodetectors," in *Conf. Lasers Electro-Optics (CLEO 1998)*, May 1998, pp. 97–98.

[16] A. Grunnet-Jepsen, A. E. Johnson, E. S. Maniloff, T. W. Mossberg, M. J. Munroe, and J. N. Sweetser, "Fiber bragg grating based spectral encoder/decoder for lightwave CDMA," *Electron. Lett.*, vol. 35, pp. 1096–1097, 1999.

[17] Z. Jiang, D. S. Seo, S.-D. Yang, D. E. Leaird, A. M. Weiner, R. V. Roussev, C. Langrock, and M. M. Fejer, "Spectrally coded O-CDMA system with four users at 2.5 Gbit/s using low power nonlinear processing," *IEEE Electron. Lett.*, vol. 40, no. 10, pp. 623–624, May 13, 2004.

[18] D. J. G. Mestdagh, *Fundamentals of Multiaccess Optical Fiber Networks*. Boston, MA: Artech House, 1995.

[19] G. Einarsson, *Principles of Lightwave Communications*. New York: Wiley, 1996.

[20] M. Razavi and J. A. Salehi, "Statistical analysis of fiber-optic CDMA communication systems—Part II: Incorporating multiple optical amplifiers," *J. Lightw. Technol.*, vol. 20, no. 8, pp. 1317–1328, Aug. 2002.

[21] C. C. Chang and A. M. Weiner, "Dispersion compensation for ultrashort pulse transmission using two-mode fiber equalizers," *IEEE Photon. Technol. Lett.*, vol. 6, no. 11, pp. 1392–1394, Nov. 1994.

Kambiz Jamshidi was born in Tehran Iran, on April 3, 1977. He received the B.S. and M.S. degrees in electrical engineering from Sharif University of Technology (SUT), Tehran, Iran, in 1999 and 2001, respectively. He is currently working toward the Ph.D. degree in the Department of Electrical Engineering at SUT.

From August 2000 to August 2001, he was a Member of Research Staff with the Advanced CDMA Research Laboratory at the Iran Telecommunication Research Center (ITRC), Tehran. From March 2002 to March 2004, he was a Member of Research Staff with Mobile Communications Division at ITRC. His research interests include optical communication systems, specifically, optical code-division multiple-access systems, applications of optical amplifiers in optical networks, and mathematical modeling of optical nonlinear devices used in communication systems.

Jawad A. Salehi (S'80–M'84) was born in Kazemain, Iraq, on December 22, 1956. He received the B.S. degree in electrical engineering from the University of California, Irvine, in 1979 and the M.S. and Ph.D. degrees from the University of Southern California (USC), Los Angeles, in 1980 and 1984, respectively.

From 1981 to 1984, he was a full-time Research Assistant at Communication Science Institute at USC engaged in research in the area of spread spectrum systems. From 1984 to 1993, he was a Member of technical staff with the Applied Research Area at Bell Communications Research (Bellcore), Morristown, NJ. From February to May 1990, he was a Visiting Research Scientist with the Laboratory of Information and Decision Systems at the Massachusetts Institute of Technology (MIT), Cambridge, where he conducted research on optical multiple-access networks. From 1997 to 2003, he was an Associate Professor and is currently a Full Professor with the Electrical Engineering Department at Sharif University of Technology (SUT), Tehran, Iran. From fall 1999 until fall 2001, he was the head of the Mobile Communications Systems group and Co-Director of Advanced and Wideband CDMA Laboratory at the Iran Telecom Research Center (ITRC), conducting research in the area of advance code-division multiple-access (CDMA) techniques for optical and radio communications systems. In 2003, he founded and and has since directed the Optical Networks Research Laboratory (ONRL) for advanced theoretical and experimental research in futuristic all-optical networks. His current research interests are in the areas of optical multiaccess networks, in particular, optical orthogonal codes (OOC), fiber-optic CDMA, femtosecond or ultrashort light pulse CDMA, spread time CDMA, holographic CDMA, wireless indoor optical CDMA, all-optical synchronization, and applications of erbium-doped fiber amplifiers (EDFAs) in optical systems. His work on optical CDMA resulted in 11 U.S. patents.

Dr. Salehi is a recipient of Bellcore's Award of Excellence, the Outstanding Research Award of Electrical Engineering Department of SUT in 2002, the Outstanding Research Award of Electrical Engineering Department of SUT in 2003, the Outstanding Research Award of SUT in 2003, the Nationwide Outstanding Research Award from Ministry of Higher Education in 2003, and the Special Nationwide Outstanding Research Award in 2004. Recently, he was introduced as among the 250 preeminent and most influential researchers worldwide by ISI Highly Cited in the computer science category. He is the co-recipient of IEEE's Best Paper Award (for a paper on "spread-time/time-hopping UWB CDMA communications systems") from the international symposium on communications and information technology in Japan in October 2004. He assisted, as a member of the organizing committee, to organize the first and the second IEEE Conference on Neural Information. Since May 2001, he has been serving as Editor for optical CDMA of the IEEE TRANSACTIONS ON COMMUNICATIONS.